Patient-Specific Finite Element Analysis of Stress Redistribution and Adjacent Vertebral Fracture Risk Following Cement Augmentation Toward Predictive Adjacent Fracture Modeling in Pre/Post-Operative Vertebroplasty for Cancer Relief

Daniel Gugig

A thesis

submitted in partial fulfillment of the

requirements for the degree of

Masters of Science

University of Washington
2026

Committee:
Dr. Avik Som
Dr. Wayne Monsky
Dr. Sandeep Vaidya

Program Authorized to Offer Degree:
Materials Science and Engineering

University of Washington

Abstract

Patient-Specific Finite Element Analysis of Stress Redistribution and Adjacent Vertebral Fracture Risk Following Cement Augmentation Toward Predictive Adjacent Fracture Modeling in Pre/Post-Operative Vertebroplasty for Cancer Relief

Daniel Gugig

Chair of the Supervisory Committee:

Avik Som

Department of Materials Science and Engineering

This thesis develops a patient-specific finite element analysis (FEA) framework to evaluate stress redistribution and adjacent vertebral fracture risk following vertebroplasty with polymethyl methacrylate (PMMA) cement. Using CT-derived DICOM data, individualized vertebral geometries and cement morphologies were segmented, reconstructed, and assembled into a tri-vertebral model subjected to physiologically relevant compressive loads. Results show that while PMMA significantly reduces strain and stabilizes the treated vertebra, it creates a stiffness mismatch that redistributes stress to adjacent levels, producing elevated stress concentrations at vertebral endplates. These stress patterns align with clinically observed adjacent-level fractures and are strongly influenced by cement volume, geometry, and spatial distribution. The study develops a framework and demonstrates the potential of CT-driven, patient-specific FEA as a predictive tool for optimizing vertebroplasty planning and reducing post-operative fracture risk.

1. Introduction

As cancer survival improves, the spine is increasingly becoming a site of secondary disease, transforming previously manageable conditions into complex biomechanical and clinical challenges. Spinal metastasis often leads to debilitating pain, spinal fracture, and large quality of life losses. Current therapy standardizes imaging of these fractures followed by temporary pain palliation via ablation and structural supplementation with bone cement. The most common readmission for these patients is adjacent bone fracture. Reduction of the risk of adjacent fracture would enable large reduction in patient suffering and current healthcare maintenance costs. Therefore, I applied in silico modeling of a trivertebral spinal section map from current patient data, cement morphologies, and predicted stress to estimate fracture risk locations when gold standard clinical polymethyl methacrylate (PMMA) cement is used. In order to model biological systems, I utilized Finite Element Analysis (FEA). At its core, FEA works by breaking down complex shapes into smaller pieces, called elements, which makes it possible to approximate how a system responds to forces, heat, or other physical effects. Because of this flexibility, FEA has been adopted across many fields, including aerospace, mechanical design, and, more recently, biomedical engineering. In aerospace, for example, FEA has enabled engineers to redesign aircraft structures such as turbine blades and wing components by identifying stress concentrations and optimizing material distribution, leading to lighter components without compromising strength or safety. Similarly, in biomedical engineering, FEA has been used to redesign orthopedic implants, such as hip replacements, by predicting how stresses are transferred between implant and bone, which has directly informed changes in implant geometry and material stiffness to reduce stress shielding and improve long-term fixation. These applications demonstrate that FEA is not simply a modeling tool, but a design-driver that enables targeted material redistribution and improved performance in both engineered and biological systems. Additionally, it allows researchers to estimate material characteristics in ways that would otherwise be difficult or even impossible to measure directly. In material science specifically, the software used in FEA has been an invaluable tool for materials characterization.

However, when modeling particular systems in the human body, such as the compression of the spinal system, difficulties begin to arise in the modeling process. Unlike metals or other traditional engineering materials, biological tissues are inherent heterogeneous composites that do not behave in simple or consistent ways. They can be highly nonlinear, anisotropic, and time-dependent, meaning their response can change depending on the direction of loading, the rate at which forces are applied, and even their past history. On top of that, no two people's "material geometry" are exactly the same. Differences in age, anatomy, health, and lifestyle all influence the mechanical properties of tissues, making it difficult to define a single "standard" model. This patient-to-patient variability is one of the biggest challenges in biomechanical modeling.

The focus of this paper is utilizing existing standard diagnostic imaging technologies to estimate the complex geometries and properties of human patient tissue, using this to create an accurate model of vertebral compression and stress transfer. Considering the biological variation of patient populations, the difficulties and limitations stated prior will require direct consideration. The goal is to make a cohesive workflow, from image conversion to future fracture prediction, that can be tailored to individual patients while also being time efficient to allow physicians to incorporate the simulated data into procedure or create a precedent for additional palliative care/risk mitigation. While FEM and FEA have been used to model compression on spinal vertebral systems, the models have traditionally been handmade using ideal geometries. These models lack the patient specific geometries to yield more curated compression data. To achieve this goal, I use FEA to identify possible sources and reasons for compression fractures extracted from CT DICOMS of fracture and cement, with stress mapping using COMSOL Multiphysics 6.4 for FEA analysis. An additional consideration in this work is the occurrence of adjacent vertebral compression fractures, where the failure of one vertebra can influence load distribution and increase the likelihood of fractures in neighboring segments. Capturing this phenomenon is essential for not only improving the predictive capability of FEA models but also it creates a possible new standard of preventative care for spinal compression failures

2. Background

Spinal compression fractures or SCFs are some of the most common fragility injuries affecting more than 1.5 million individuals annually in the United States alone (1). They are usually a result of spinal vertebrae becoming osteoporotic either due to aging, trauma or spinal metastases (1). Osteoporotic vertebral fractures account for approximately 700,000 new cases each year and are a major contributor to pain, reduced mobility, spinal deformity, and diminished quality of life in elderly patients (2). Bone cements, such as the most commonly used PMMA, have become a standard minimally invasive option for managing spinal compression fractures in recent decades. In procedures such as vertebroplasty and kyphoplasty, these materials help re-establish structural stability and most importantly ease pain (3). By stabilizing the fractured vertebra and reducing micromotion, cement augmentation directly targets one of the main sources of ongoing pain (4). With an aging population and rising rates of osteoporosis and spinal metastases, these cement-based interventions are expected to become even more central to vertebral fracture care.

Due to the sensitivity of the spinal column, direct imaging of the procedure and fracture are necessary, primarily being clinically conducted by interventional radiologists (IR). IR assess patients suspected of vertebral compression fractures via clinical evaluation and advanced imaging, primarily CT. CT uses volumetric datasets consisting of spatially registered cross-sectional slices in DICOM format (5). Considered factors include characterization of pain, recent trauma, functional decline, and risk factors such as osteoporosis or malignancy (6,7). CT is frequently used when magnetic resonance imaging is contraindicated or when detailed visualization of cortical disruption, retropulsion, or complex fracture morphology is required, and it is also appropriate in patients with multiple or previously treated fractures (6). In cases where malignancy is suspected additional modalities such as fluorodeoxyglucose positron emission tomography (FDG-PET), bone scintigraphy, or image-guided biopsy may be necessary (4,8). An interventional radiologist can also test for mechanical stability by using the Spinal Instability Neoplastic Score (SINS), a classification system aggregating these other findings. The SINS score is calculated by assigning numerical values to six categories: location of the lesion (0–3 points), mechanical

pain (0–3 points), bone lesion type (0–2 points), spinal alignment (0–4 points), degree or severity of vertebral collapse (0–3 points), and extremity involvement such as if pedicles or facet joins are involved in the collapse (0–3 points). The cumulative score ranges from 0–18, where scores of 0–6 indicate stability, 7–12 indicate potential instability, and 13–18 indicate spinal instability requiring urgent surgical evaluation (**Table 1**). Although SINS does not directly quantify peak mechanical stress, there is a positive relationship between increasing SINS score and increased loss of vertebral load bearing capability (9). For the purpose of this study, I will be doing a compressive model on a patient with a SINS score of 13-18.

Table 1. Summary of SINS score and the considerations needed prior to operation. (9)

Total Score	Stability Classification	Clinical Implication
0–6	Stable	Nonoperative management; radiotherapy alone often sufficient
7–12	Potentially unstable	Surgical or interventional consultation recommended
13–18	Unstable	Mechanical stabilization required

A supplementary method of categorizing the stability of a patient's spine is the use of DEXA or Dual-Energy X-ray Absorptiometry. This is a quantitative imaging technique that uses two X-ray photon energies to measure bone mineral density, density often being decreased in older patients or peritumoral (10). Low bone mineral density increases the likelihood of cement leakage and fragility fractures during tool implantation (12). The data provided is recorded as T-scores and Z scores and it is an objective assessment of skeletal integrity that can inform an interventional radiologist of the potential risk of performing a vertebroplasty or kyphoplasty (11,12) (**Figure 1)**. DEXA, in conjunction with MRI and CT, offers a reference standard for diagnosing osteoporosis over a 15-minute procedure (13).

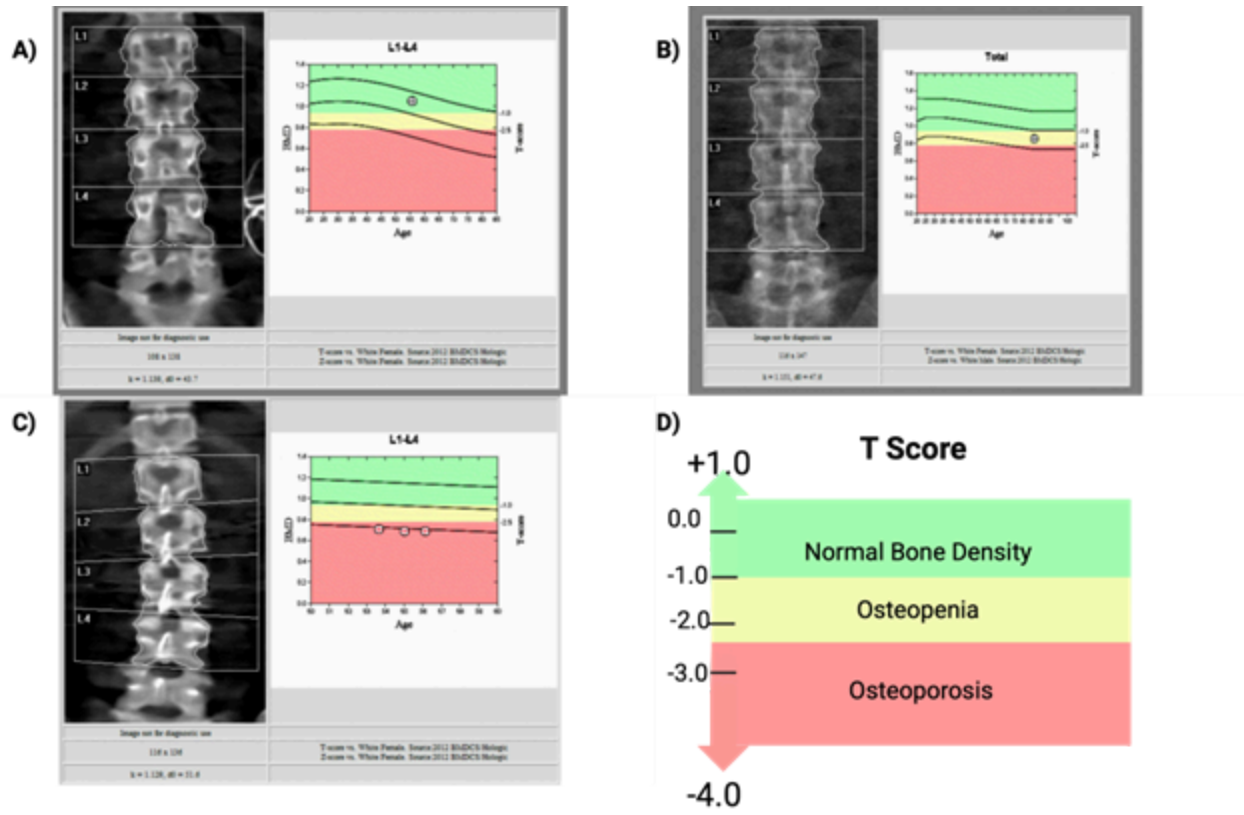

Figure 1: A) DEXA scan of a healthy vertebrae B) DEXA scan of osteopenia vertebrae C) DEXA scan of Osteoporosis D) A T-score for bone density comparing the tested bone density to that of a young adult of the same sex. Osteopenia is lower than normal bone density but not quite osteoporotic. Images of DEXA provided by the University of Washington Department of Radiology

As bone cement offers mechanical stabilization of osteolytic lesions, particularly in the spine, percutaneous vertebroplasty has become the standard palliative treatment (**Figure 2**). Typically using PMMA-based cements they have demonstrated excellent efficacy in stabilizing affected vertebral bodies (14,15). Clinical series report >80% of patients experience significant pain relief within 48–72 hours of augmentation (16,17). In combination with ablative therapies, vertebral augmentation has demonstrated lifelong local control and biomechanical reinforcement with many patients never needing additional spinal readjustments (18).

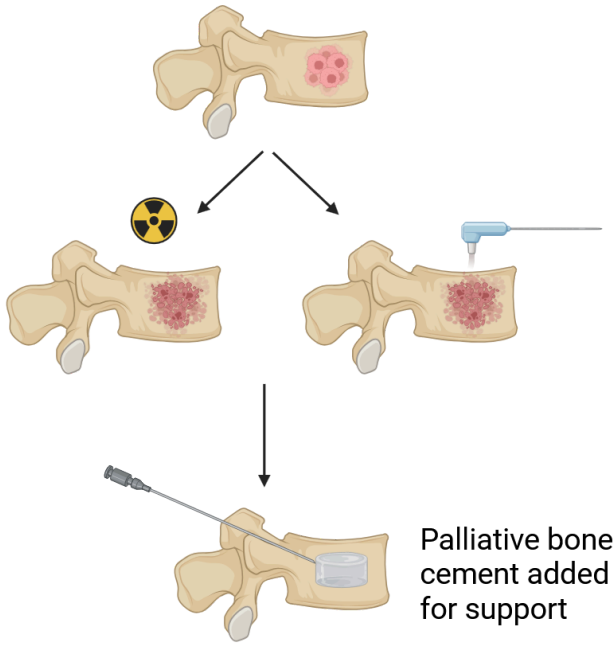

Figure 2: Image depicting the process of first radiating or ablating a metastatic lesion site before placing the cement implant

Those that do have complications usually arising from 55 days to 6 months after implantation and are usually as a result of a cascade of issues related to patient history (18).

Osteoporotic vertebral compression fractures are particularly challenging because the compromised vertebral structure provides 30%-75% less support than healthy vertebrae. Interventions such as

vertebroplasty and kyphoplasty rely on PMMA to re-establish mechanical stability (19). However, while PMMA's inherently high stiffness does shield the injured vertebra, it focuses stresses to adjacent bone, which will predispose patients to adjacent-level fractures (20). To mitigate these issues, newer PMMA formulations have been developed to match the material properties of either osteoporotic or healthy bone (20).

Formulations of PMMA can vary in their inherent material strength, ranging in elastic modulus from 1,700–3,700 MPa and compressive strength from 85–114 MPa. Osteoporotic trabecular bone demonstrates a far lower modulus of 10–900 MPa and compressive strength of 0.1–15 MPa (14). Materials science has shown similar mechanical mismatch creates elevated stress at the interface due to stress shielding, a fact seen in elevated adjacent-level fracture data (14). By disproportionately stiffening the treated level, PMMA shifts mechanical loads to neighboring segments, which may accelerate structural damage and contribute to adjacent-level fractures, particularly in already osteoporotic or metastatically weakened bone.(21,22) Clinical reports estimate the incidence of adjacent-level fractures to range from 12% to 52%, often occurring within the first few months post-procedure (23).

To reduce this risk, investigators have developed low-modulus PMMA formulations by introducing controlled porosity often achieved by adding aqueous components such as sodium hyaluronate. These modifications have produced cements with porosities up to 56%, decreasing the Young's modulus from 930 MPa to 50 MPa and the yield strength from 39 MPa to 1.3 MPa, thereby aligning more closely with the mechanical profile of osteoporotic bone (24). Such adjustments mitigate the mismatch and significantly lower the incidence of adjacent fractures (25). The corresponding biomechanical properties governing thoracic and lumbar spinal behavior are summarized in **Table 2**. While these formulations attempt to reach natural bone characteristics, they face regulatory and clinical scrutiny, as any modification must maintain the compressive strength of PMMA within ASTM F451 or ISO 5833 standards as required for FDA compliance. These require acrylic cements to reach a minimum load bearing threshold of 70 MPa.

Table 2. Biomechanical parameters of thoracic and lumbar vertebrae. (26)

Part of Spine	Volume (cm^3)	Compressive Force (MPa)	Longitudinal Modulus (MPa)	Circumferential Modulus (MPa)	Fracture Toughness (MPa√m)
Thoracic	15.0	3.8	38.1	21.2	3.5
Lumbar	35.2	4.0	36.6	12.2	6.6

Cement augmentation can also alter the physiological environment of the spine, leading to stress shielding of adjacent vertebrae. Furthermore, the risk may be exacerbated by excessive cement volume or leakage, which can alter local biomechanics and increase stress concentrations at adjacent endplates (27). Beyond these biomechanical concerns PMMA cement presents several additional limitations that restrict its broader application. Notably, PMMA is biologically inert and exhibits poor osteointegration, which limits its long-term integration with host bone and makes it less suitable for younger patients where biological remodeling is desired (28). Additionally, PMMA is non-degradable and lacks bioactivity, preventing it from supporting new bone formation or adapting to changes in the surrounding environment over time (28).

An additional limitation is its inability to address underlying pathological processes, particularly in cases involving spinal tumors. While PMMA can provide immediate structural stabilization, it does not possess therapeutic capability to treat residual tumor tissue, meaning disease progression may continue despite mechanical reinforcement (29). The polymerization process of PMMA also introduces risks associated with its exothermic reaction; temperatures during curing can exceed 70 °C, potentially leading to thermal necrosis of surrounding bone and damage to adjacent neural structures (30,31). This heat generation, combined with the release of unreacted monomers, has also been associated with cytotoxic effects and compromised local tissue viability (28,31).

Furthermore, the risk may be exacerbated by excessive cement volume or leakage, which can alter the local biomechanics (32). FEA and biomechanical studies have demonstrated that PMMA injection

increases the stiffness of the treated vertebra, which may contribute to a mismatch in compliance between augmented and adjacent untreated vertebrae, predisposing them to subsequent failure (23,32,33) Considering the redistribution of stress, the ability to directly predict how certain materials and geometries can affect the final vertebral stress distribution is essential to predicting patient outcomes. Collectively, these limitations highlight that while PMMA remains a clinical standard, its mechanical and biological drawbacks remain significant considerations in both clinical application and the development of next-generation bone cements.

Several groups have modeled the Vertebral system using finite element analysis in an attempt to determine this stress shielding/focusing effect. The research team led by Dr. B.T Dickey group created a simplified model of a single L4 vertebrae (**Figure 3**) with an outer cortical bone shell (displayed in light blue) with an inner trabecular bone pocket (displayed in yellow) and finally the "implant" (displayed in grey). The implant had a customizable Poisson ratio and density to fit the characteristics of a suite of materials. As they tested they found that the acrylic cement or PMMA had the least amount of stress remaining within the interior of the vertebrae implying that the stress was transferred through the cement and out of the simulated system (34). However, this group related the Dr. B.T Dickey's study was published in 2011 and the researchers themselves explained that they took large simplifications necessary to enable them to keep the scope of the investigation possible (34). Since then, FEA software has advanced dramatically and the use of more complicated trivertebral models have become standard practice.

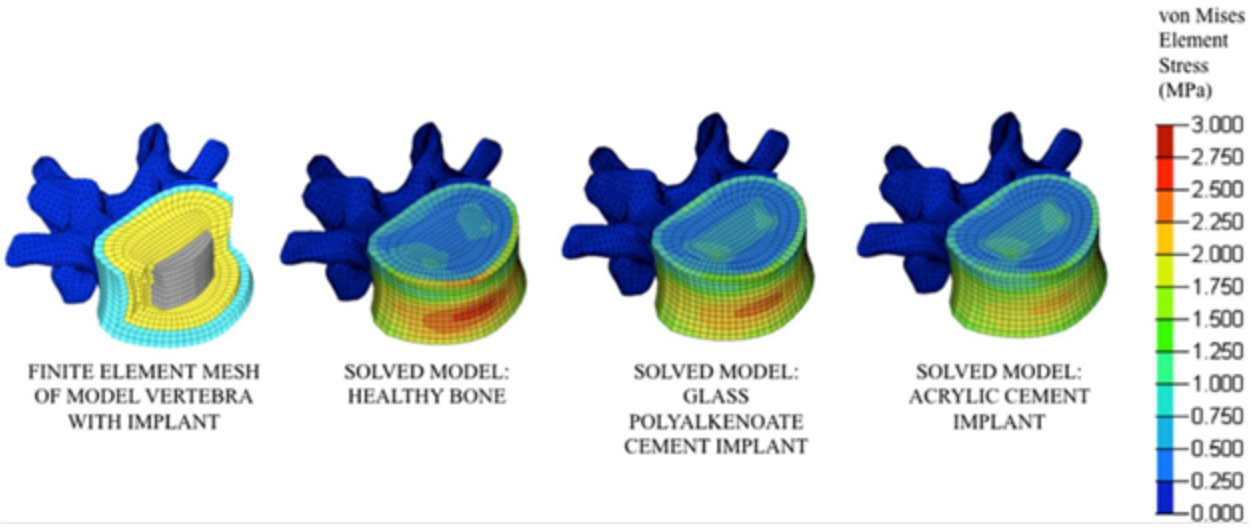

Figure 3: Finite element analysis of the von Mises element stress within a vertebrae simulated with healthy bone, glass polyalkenoate cement, and PMMA (34) The von Mises element stress is a scalar that approximates the value in which a material will yield or permanently deform. Reproduced under Creative Commons License

A more complex trivertebral model (**Figure 4**) was developed by Chabarova, including calculation of endplates, stress distribution into the pedicle, and importantly the distribution of stress from one vertebrae distributed to adjacent vertebrae (35). The finite element results demonstrate that osteoporosis significantly alters load transfer through the lumbar spine, increasing deformation and reducing mechanical stability. Under compressive loading, the model shows that reduced trabecular bone density shifts a greater proportion of load to the cortical shell, leading to higher stress concentrations and earlier onset of plastic deformation. This redistribution of forces not only weakens the vertebral body but also affects how loads are transmitted across the intervertebral discs into adjacent vertebrae. As a consequence, disc deformation increases by more than 30% in osteoporotic cases, even when disc properties remain unchanged, indicating that vertebral degeneration alone can amplify disc strain. The model further shows that disruption of the trabecular cortical interface (simulated as loss of bonding) has a particularly strong effect on load transfer pathways. In these cases, the ineffective transmission of forces through the vertebral body results in localized instability and increased shear and bulging in the discs, reflecting a higher computational “load transfer penalty” across segments. This manifests as increased disc shearing and greater vertebral deformation, indicating that forces are less efficiently distributed and instead concentrated at structural weak points (35).

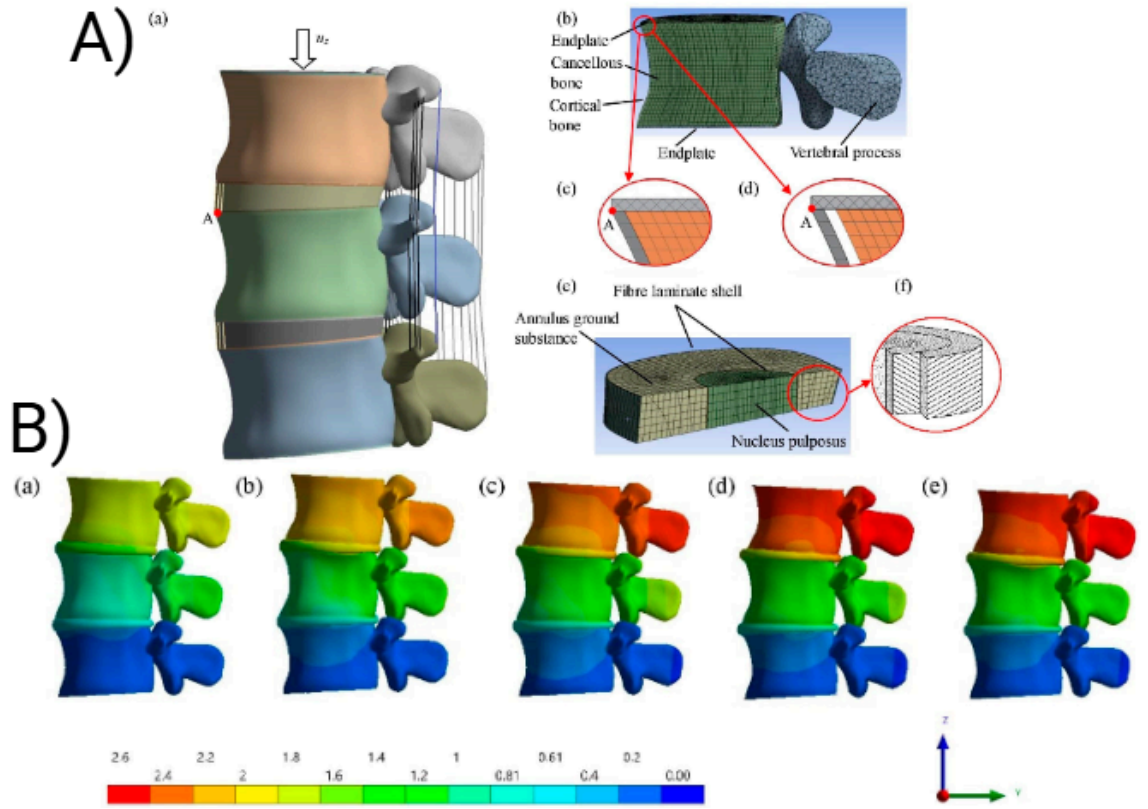

Figure 4: Finite element analysis of the total displacement of vertebrae in a tri vertebrae system with constant load displacement of 2.5 mm. A) The set up dimension, mesh, and shell parameters of the system. (a) describes the force direction and overall elastic geometry. (b)(c)(d) Visually show the mesh differentiation for the cortical and trabecular bone and how the geometry at some angles contains gaps in free space.(e)(f) are the mesh and geometry for the cartilage or middle places between vertebrae. B) is a model of the system where (a) has a normal bone density and decreases (b)-(e) with e having the lowest bone density simulating a degenerated vertebral disc. (35)

For compression testing, boundary conditions are typically defined by constraining the bottom most vertebra while applying an axial compressive load to the top most vertebra, thereby replicating physiological activities such as standing or forward bending. This setup allows for the evaluation of mechanical outputs, including vertebral displacement, intervertebral disc deformation, intradiscal pressure, and stress distribution throughout the spinal segment (36).

3. Methodology

The primary distinction between previously discussed models and the model proposed herein is the source of the underlying geometric representation. In earlier studies, models were typically constructed manually

using generalized anatomical geometry derived from real-world measurements to set constraints. While this approach allows for flexibility in adjusting parameters and exploring a wide range of conditions, it lacks the level of specificity required to accurately capture individual anatomical variations, limiting its applicability for patient-specific palliative care. In contrast, the model developed in this thesis is based on extracted geometries from anonymized patient CT data (**Figure 5**), enabling an individualized representation of the lumbar spine.

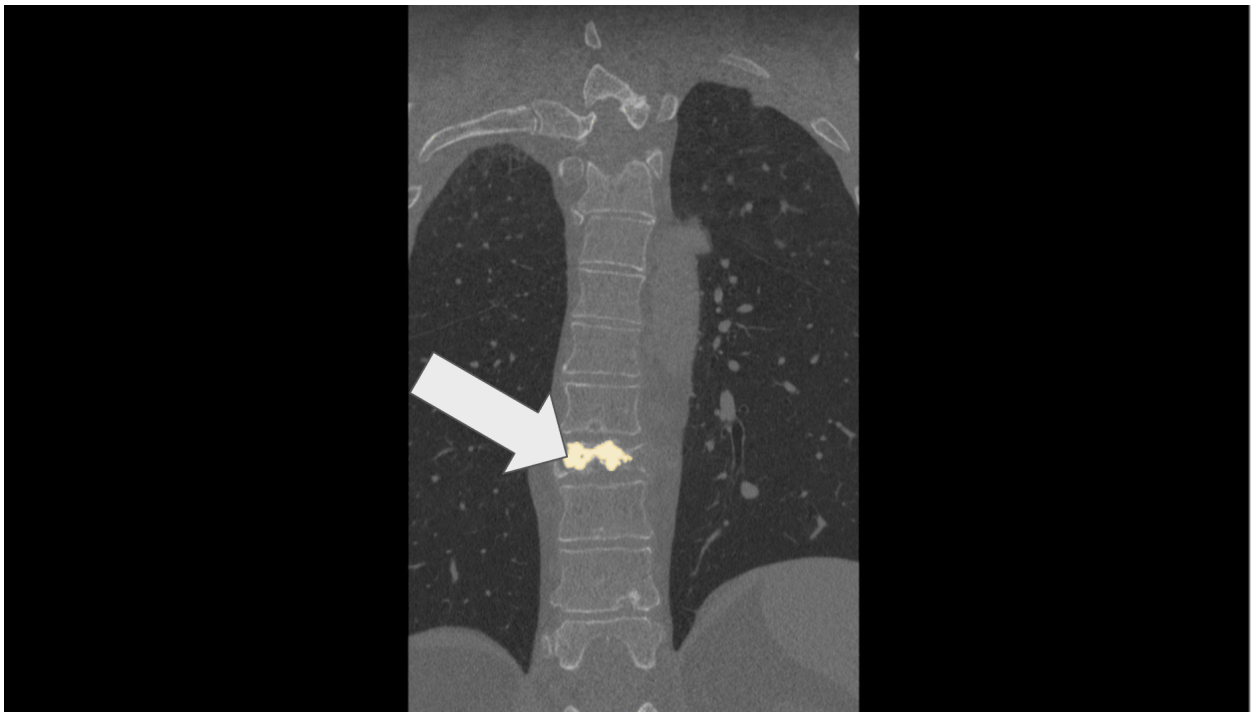

Figure 5: Example CT scan of a patient post vertebroplasty. The vertebrae in question suffered a compression fracture and was filled with approximately 7 mL of PMMA bone cement. The bone cement is identified with a white arrow. CT scan given by University of Washington Department of Radiology.

When a patient is first admitted into the hospital for an ailment involving the spine preliminary investigations are done using CT, MRI, and DEXA. Prior to extraction for research use, imaging studies were processed through the institution's clinical data management infrastructure to remove protected health information (PHI). Patient identifiers contained within DICOM metadata, including names,

medical record numbers, accession numbers, dates of birth, and other direct identifiers, were either removed or replaced with unique study-specific research identifiers. Any linkage between research identifiers and patient identities was maintained separately on secure institutional servers accessible only to authorized study personnel. De-identified imaging datasets were subsequently exported for analysis in accordance with institutional review board (IRB) requirements and applicable Health Insurance Portability and Accountability Act (HIPAA) regulations.

Using this data, a 3D model can be extracted of not only the spine but of the bone cement as well. For the purpose of 3D model ex traction, the primary imaging technique used will be CT for its superior high spatial resolution and strong contrast for osseous anatomy. CT is governed by the Hounsfield scale for imaging which describes how much a tissue attenuates X-rays by bases it relative to water and air. This scale is the basis for detecting vertebrae that have been subject to compression failures, cement implantation, and adjacent fractures.

Using a scan **(Figure 4)**, a vertebra with bone cement can be isolated by manipulating the Hounsfield scale to section away connecting tissue and fluid while also preserving the geometry needed to conduct compression tests within FEA. This process was carried out in 3D Slicer (version 5.8.1), which provides tools for threshold-based segmentation and 3D model extraction. By carefully adjusting the Hounsfield Unit (HU) thresholds, different material types within the CT scan can be separated: soft tissues and fluids typically fall within a lower HU range (approximately −100 to +100 HU), while trabecular bone ranges from roughly +150 to +700 HU, and cortical bone exceeds +700 HU. Bone cement, depending on its composition, typically appears at higher radiodensity values, often above +1000 HU. To extract the vertebra accurately, an initial thresholding step is applied to exclude low-density materials such as surrounding soft tissue, fat, and fluid. A commonly effective threshold range for isolating bone structures is approximately +150 HU to +2000 HU. When bone cement is present, a higher threshold can help distinguish it more clearly from trabecular bone, allowing selective segmentation of both regions if needed. After the selected vertebra is isolated, region-based tools can be used to further section it from adjacent anatomical structures, ensuring that only the target vertebra remains. In SOLIDWORKS,

repairing a broken mesh model typically involves a sequence of tools that align closely with operations like removing small disconnected regions, trimming boundaries, and masking areas of interest. The process often begins with the Mesh Prep Wizard (ScanTo3D), which can automatically detect and eliminate small, isolated mesh fragments (noise), ensuring that only meaningful geometry remains. From there, domain boundaries can be refined using tools such as Cut With Plane, Trim, or Split, which allow you to section the mesh and isolate the specific anatomical region, such as a single vertebra, from surrounding structures. To further isolate the vertebral body and relevant processes, SOLIDWORKS provides mesh selection tools (like lasso or paint selection) and segmentation capabilities, enabling users to effectively "mask" unwanted regions by selectively hiding or deleting facets. Once the desired region is isolated, issues such as holes or damaged geometry can be corrected using Mesh Repair and Fill Holes, which restore continuity and create watertight surfaces. After structural repairs, refinement tools like Smooth Mesh, Remesh, or Decimate help improve surface quality and optimize triangle distribution. Finally, the cleaned mesh can be converted into usable CAD geometry through the Surface Wizard or by creating a solid body, enabling further design, simulation, or analysis.

This step is significant for keeping a majority of the unique structural features critical for mechanical analysis, specifically endplate shape and vertebrae height. Once segmentation is complete, the isolated vertebra can be converted into a 3D surface model. The extracted geometry is then exported as an STL mesh file compatible with most FEA software. This file represents a triangulated surface mesh that captures the patient-specific morphology of the vertebra, including the distribution and integration of bone cement. As a result, the model captures patient's unique geometry, with meshing and surface characteristics directly from the CT data, enabling highly accurate and individualized biomechanical simulations (**Figure 6**).

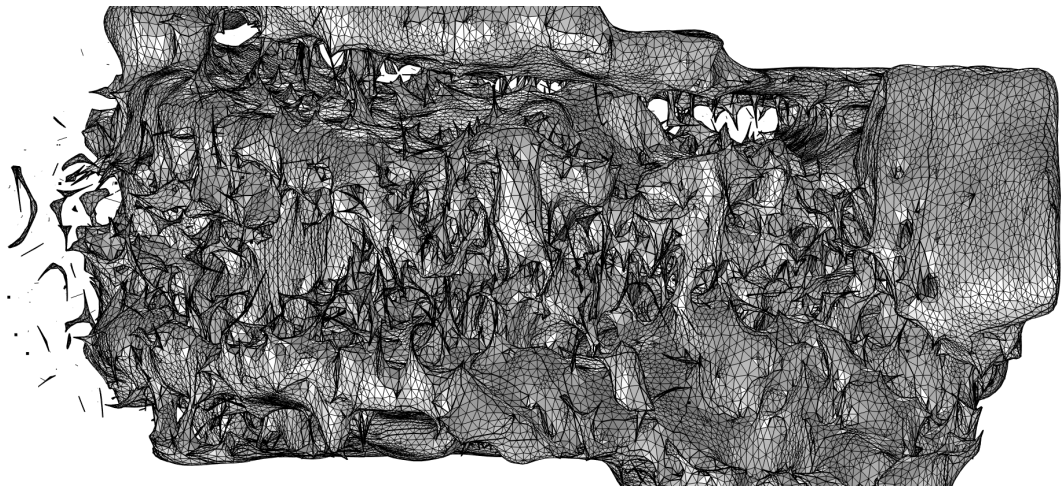

Figure 6: A side view of the affected vertebrae containing bone cement visualized within COMSOL. The many missing meshes, straight through holes, and floating bits of computation are uncomputable domains that require polishing and resizing in order to properly be used in FEA software

A primary issue with patient DICOMs is the inherent complexity that comes with modelling a true geometry. Most handmade models make numerous assumptions to reduce the amount of artifacting while also reducing the mesh size to make computation possible. Even when a mesh is successfully generated and can be viewed in 3D space, the resulting extracted vertebra may still be unusable because of full‑thickness holes, irregular voids, and artifact particles introduced during digital extraction. In healthy individuals, bone segmentation is relatively straightforward because bone density is more uniform; however, in patients with metastatic disease or osteoporosis, the reduced bone density makes isolation of a clean uniform structure difficult. As a result, the segmented vertebra often contains discontinuities or non‑physiologic geometries that cannot be meshed or computed reliably.

To mitigate this I placed the extracted 3D shapes into SOLIDWORKS Education edition 2025 SP2.0 as an STL file. The meshed geometry is unique to the patient and in order to maintain the patient specificity of the model careful reconstruction is conducted within SOLIDWORKS. This involves creating small meshed structures to individually fill in holes and reconstitute vertebral walls and endplates. This process can be time intensive but careful considerations need to be made in order to maintain the models unique characteristics. From this newly constructed model it can then be imported to

COMSOL Multiphysics 6.4 for FEA. While in COMSOL, the physical data of the model can be specifically manipulated by using known material properties in conjunction with CT and patient data to construct a cohesive model that closely resembles the patient's original spinal conditions. While the resulting geometries are not perfect copies of real patient vertebrae and cement, these assumptions are particularly important for the construction of the pedicle which is needed for proper stress distribution once the compression test is conducted. From the HU and cleanup methods above, the treated and adjacent vertebrae are extracted from patient DICOMs.

Using these, a stress distribution FEA model was generated using parameters meant to mimic a healthy control, an osteoporotic model, and an osteoporotic bone with a cement implantation. Using COMSOL STL Import 1 - Repairing and Combining STL Files as a guide for merging different meshes into one system, a tri vertebrae model can be created (**Figure 7**) that additionally models the cartilage in the spinal system, a system often overlooked due to the added mechanical considerations needed to properly simulate. The vertebrae were labeled V3, V2, and V1 for the top, middle, and bottom vertebrae respectively. Fitted into the spinal system were three sets of bone cement shapes (**Figure 8**). Geometry 1 is the original bone cement shape in its original orientation at, Geometry 2 is a bone cement shape derived from a different patient's CT scan who also underwent cement implantation to treat a compression fracture, and Geometry 3 is the ASTM cylinder. Additionally the stress of the vertebral system is measured graphically by taking a 1D vertical cut line through the center of all three vertebrae (**Figure 9**).

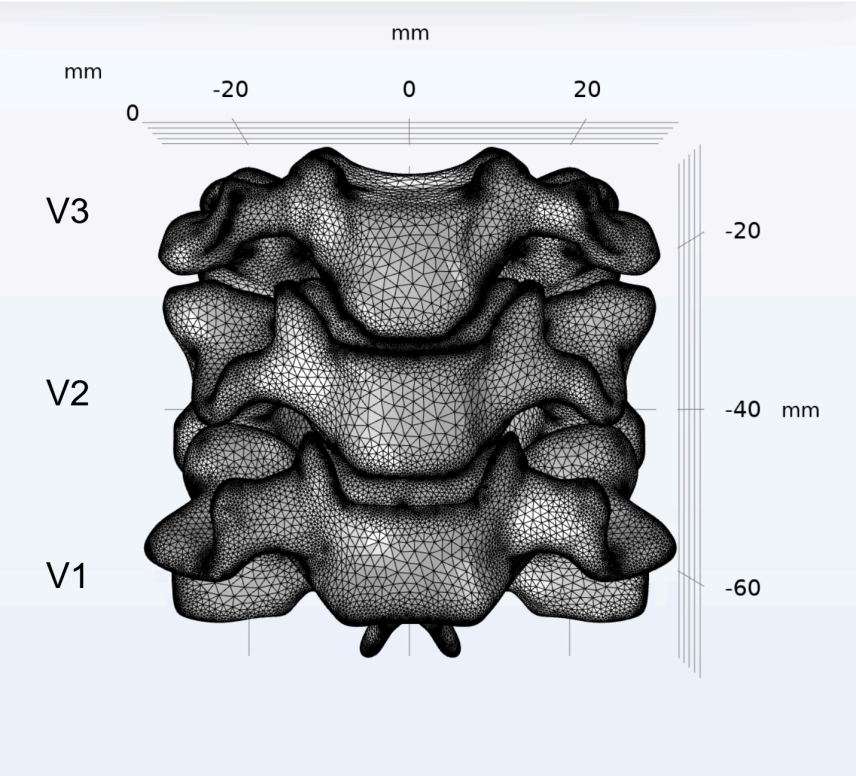

Figure 7: Tri vertebral arrangement meshed together in COMSOL. The extracted STL file was imported into COMSOL and all mesh defects corrected, resulting in a reconstructed, properly meshed voxel model for FEA analysis. The model has had each vertebrae renamed to V1 for the bottom most component, V2 for the affected vertebrae, and V3 for the top most vertebrae.

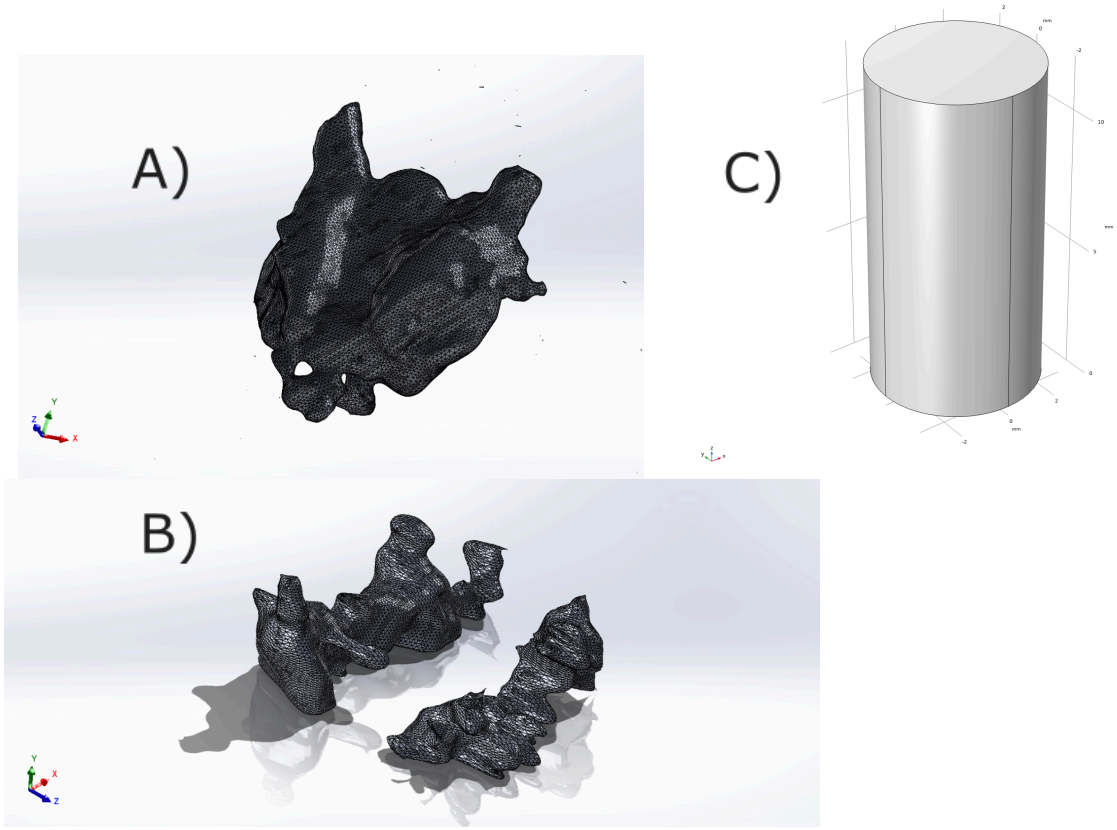

Figure 8: Three cement geometries. A) Geometry 1 extracted from the original patient visualized in SOLIDWORKS. B) Geometry 2 extracted from a different patient visualized in SOLIDWORKS. C) ASTM cylinder visualized in COMSOL

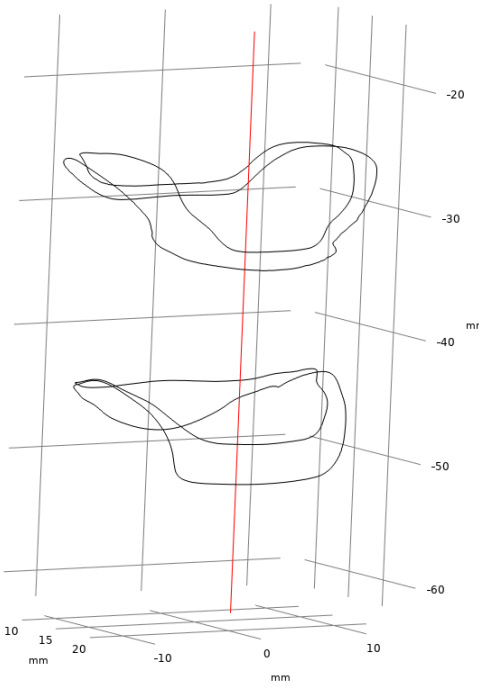

Figure 9: Cut line used to gather the internal stresses and strain

Table 3. Spinal properties for the tri vertebrae model. Values bolded were values derived from patient specific CT data and values in parentheses were used in the compression study

Material	Young's modulus [E] (GPa)	Poisson's ratio (ν)	Peak strength (yield) (σ_Y) (MPa)	Fracture energy (area) [J/m²]	Ref.
Healthy cortical bone	10–20 **(15)**	0.30–0.35 **(.30)**	100–150 **(120)**	~1,000–5,000 **(3550)**	[37,38,39]
Osteoporotic bone	1–8	0.20–0.35 **(.25)**	20–80 **(25)**	~200–1,500 **(855)**	[40,41,42]

	(3)				
Intervertebral disc cartilage	0.1–10 (.4)	0.40–0.49 (.45)	2–10 MPa (4)	~100–1,000 (500)	[43,44,45]
PMMA bone cement	2–3 **(3)**	0.30–0.35 **(.30)**	70–100 MPa **(100)**	~100–500 **(200)**	[46,47,48]

The array of forces being tested were tested in a suite to get a range of three physiological circumstances for the possible fracture. The three scenarios were standing, walking, and a small impact roughly replicating a 3ft jump. In the table the loads and parameters are described

Table 4. Load parameters for different scenarios for compression

Activity	**Pressure (MPa)**	**Ref.**
Standing	~0.5 MPa	[36]
Running	~1.2	[36]
3 ft Impact	~3.0 MPa	[49]

4. Results

Using the extraction method described above, the vertebral geometries for a single patient case (n = 1) with variable vertebral implant sizing were successfully generated following mesh repair, domain creation, and segmentation in COMSOL. Due to the limitations of IRB approval for the research of patient data only one dataset was processed, this makes variability in model generation limited; however, the workflow demonstrated consistent reconstruction of domains suitable for quantitative analysis. The resulting anatomical measurements showed a gradual increase in size from the superior to inferior levels, consistent with expected lumbar trends (50) (**Table 5**). The values extracted fall within reasonable anatomical ranges for cervical vertebrae and provide a baseline for evaluating how well the reconstructed geometries replicate real morphological characteristics.

Table 5. Extracted data for the vertebrae

Property	**V1**	**V2**	**V3**
Height (mm)	28	24	22
Volume (mm^3)	28,118	24,302	22,490

In addition to the bone geometry, the bone cement region was also extracted from the CT imaging data. The workflow demonstrated consistent identification of high-density regions corresponding to PMMA cement and successful conversion into a volumetric domain suitable for analysis (**Table 6**) The reconstructed cement volumes across the treated vertebral levels showed values in the range of 339 –7000 mm^3, depending on implant spread and fill pattern within the affected vertebrae vertebra. Material density

was consistent with typical PMMA values (~1.1–1.2 g/cm³), reflecting the relatively uniform radiodensity observed in the segmented CT regions. A key modeling consideration was the spatial distribution of cement relative to the vertebral body, particularly the projected surface area in the transverse (YZ) plane, which directly influences load transfer and stress shielding behavior. In this case, the cement occupied an estimated 25–40% of the vertebral cross-sectional area when viewed along the spinal axis, indicating partial load-sharing between native bone and implant. This distribution is important, as increased projected area coverage can lead to greater stress shielding of surrounding trabecular bone, potentially affecting long-term biomechanical response.

Table 6. Data of each bone cement geometry extracted from CT scan

Property	**Geometry 1**	**Geometry 2**	**Geometry 3**
Height (mm)	10	7	12
Volume (mm^3)	7000	5530	339

Once assembled, the model was run under uniform compressive loading down the spinal column. Using heat map visualization of the stress (**Figure 9**), it is apparent that stress accumulates at the intervertebral interfaces, particularly at the conjoined regions between adjacent vertebrae. This effect was most pronounced following cement implantation, where the mechanical mismatch between the high-stiffness PMMA and the surrounding osteoporotic bone altered load sharing pathways across the vertebral

segment. As a result, stresses that would typically be dissipated within the trabecular structure of the central vertebra were instead redistributed toward adjacent levels causing spikes in stress that range from .4MPa-.7MPa from the original load value.

The tri vertebral system demonstrates a distinct stress redistribution pattern within the implanted vertebra, coupled with stress amplification in neighboring segments. As compressive forces increase from 0.5-5 MPa, elevated stresses are observed at interfaces with V2, the top most endplate of the lower vertebra (V1) and at the inferior endplate of the upper vertebra (V3) relative to implant free conditions. This reflects the literature stress shielding literature, load being transferred away from the augmented vertebra. However, this focuses additional stress into the intervertebral interfaces. While the presence of the implant produces a more diffuse stress field within V2, the overall magnitude of stress across the system is increased relative to the non-implanted case which coincides with the spikes in stress seen at the interfaces of V1 and V3 with V2 (**Figure 9**).

This indicates that although the implant reduces local deformation within the treated vertebra (V2), it does so at the expense of increased global load transfer through the tri-vertebral system. It is important to note that in this model the bottom vertebra (V1) is constrained as a fixed boundary condition, while the compressive load is applied to V3, which contributes to the elevated stress response observed at the superior segment. Examination of peak stress concentrations shows localization to the inferior endplate of the V3 vertebra and at discrete regions of structural intersection within V3. These peaks correspond to areas of high load transmission from the cement-augmented segment (**Figure 10**) and align with clinically observed fracture locations at the adjacent superior endplate. Spatially, the stress amplification is not uniformly distributed across the vertebral body but instead reflects the geometry of the injected cement within V2. Regions of V3 that are aligned with load paths extending from the cement mass show greater stress concentration, suggesting that load transfer occurs preferentially through reinforced pathways, while adjacent regions lacking cement support experience relatively reduced transmission. This indicates that stress propagation is influenced by the projected distribution of cement in the transverse plane, where

partial coverage creates heterogeneous “columns” of stiffness rather than a fully uniform load-bearing structure. Within V2 itself, the cement produces a more homogeneous internal stress field, but this homogenization directly contributes to sharper stress gradients at the V2–V3 interface, reinforcing the tradeoff.

In contrast, within the implanted vertebra, the stiffening effect of the cement produced a more uniform stress distribution, effectively reducing localized stress concentrations within the osteoporotic bone matrix. This homogenization of stress within V2 reflects the intended stabilizing effect of vertebroplasty; however, it simultaneously contributes to increased stress gradients at adjacent levels.

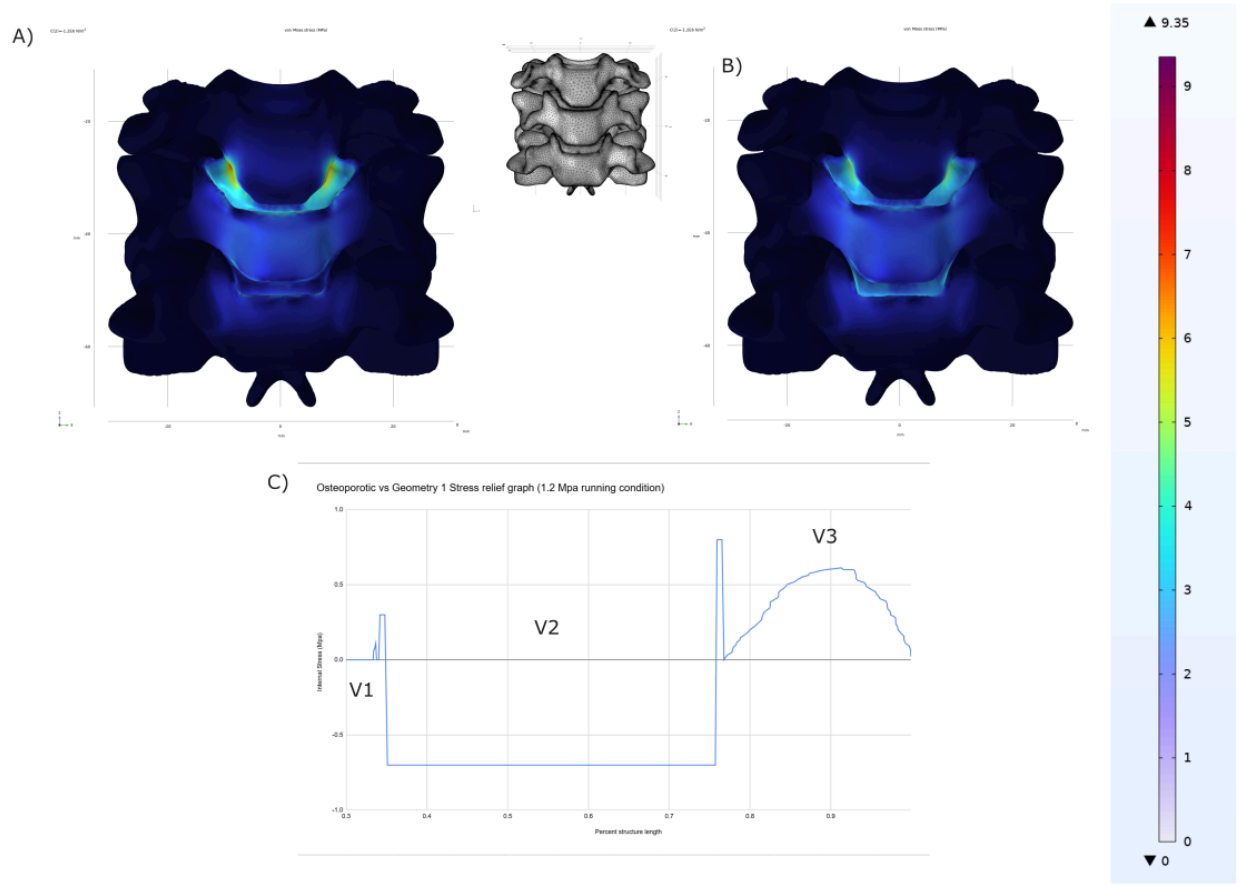

Figure 9: The stress concentration across the trivertebral system mapped across an osteoporotic central vertebrae with and without cement implantation A) Is the 3D visualization of the stress concentration of an osteoporotic central vertebrae B) Is the 3D visualization of the stress concentration of the same affected vertebrae with a cement implant with geometry 1. C) A graph detailing the summation of the internal stresses of the system with implant minus the internal stresses of the system without implant. The sections are divided by V1 (the bottom vertebrae), V2 (the affected osteoporotic vertebrae), V3 (The top vertebrae

where the boundary load is administered. Negative stress details an area in which stress is relieved from the vertebrae and positive stress indicates a region of increased stress. All data was gathered by loading the top vertebrae with 1.2 MPa in the -z direction

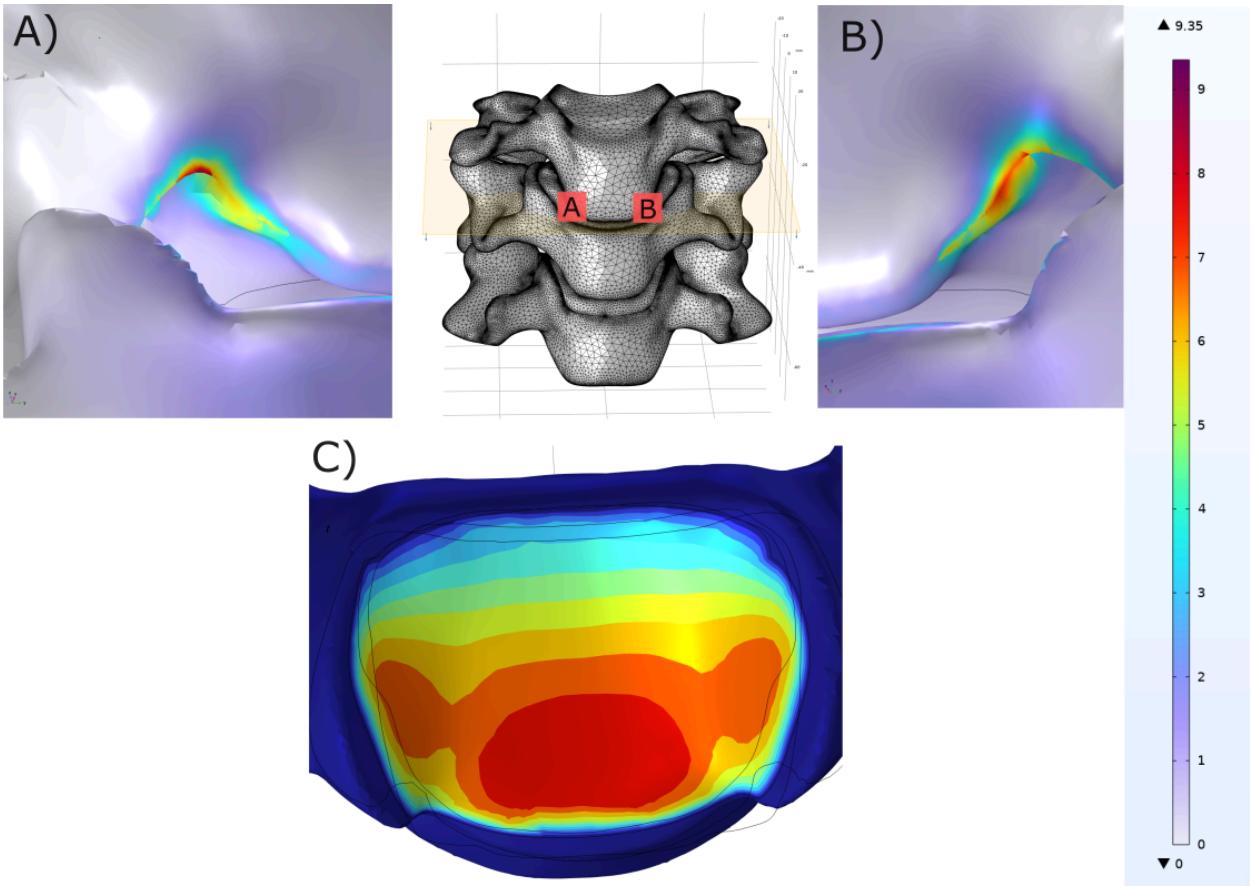

Figure 10: All data was gathered by loading the top vertebrae with 1.2 MPa in the -z direction while the implant with geometry 1 was inserted into the V2 vertebrae In the middle the total meshed structure with a slice plane to analyze the bottom of vertebrae V3. A) One of the areas with the most stress concentration on the right side of the V3 vertebrae. B) One of the areas with the most stress concentration on the left side of the V1 vertebrae. C) Stress map of the bottom end plate of the V3 vertebrae.

Under the same load of 1.2 Mpa the strain data showed the cement provided a drastic reduction of the V2 strain from a magnitude of 30-40 to 4-5 (10x reduction, **Figure 11**). This is a substantial decrease in vertebral compression that is expected of an implanted cement. An important distinction to note is that while strain may be reduced in the vertebral system post implantation the overall stresses and concentration of stresses can still increase relative to normal osteoporotic bone.

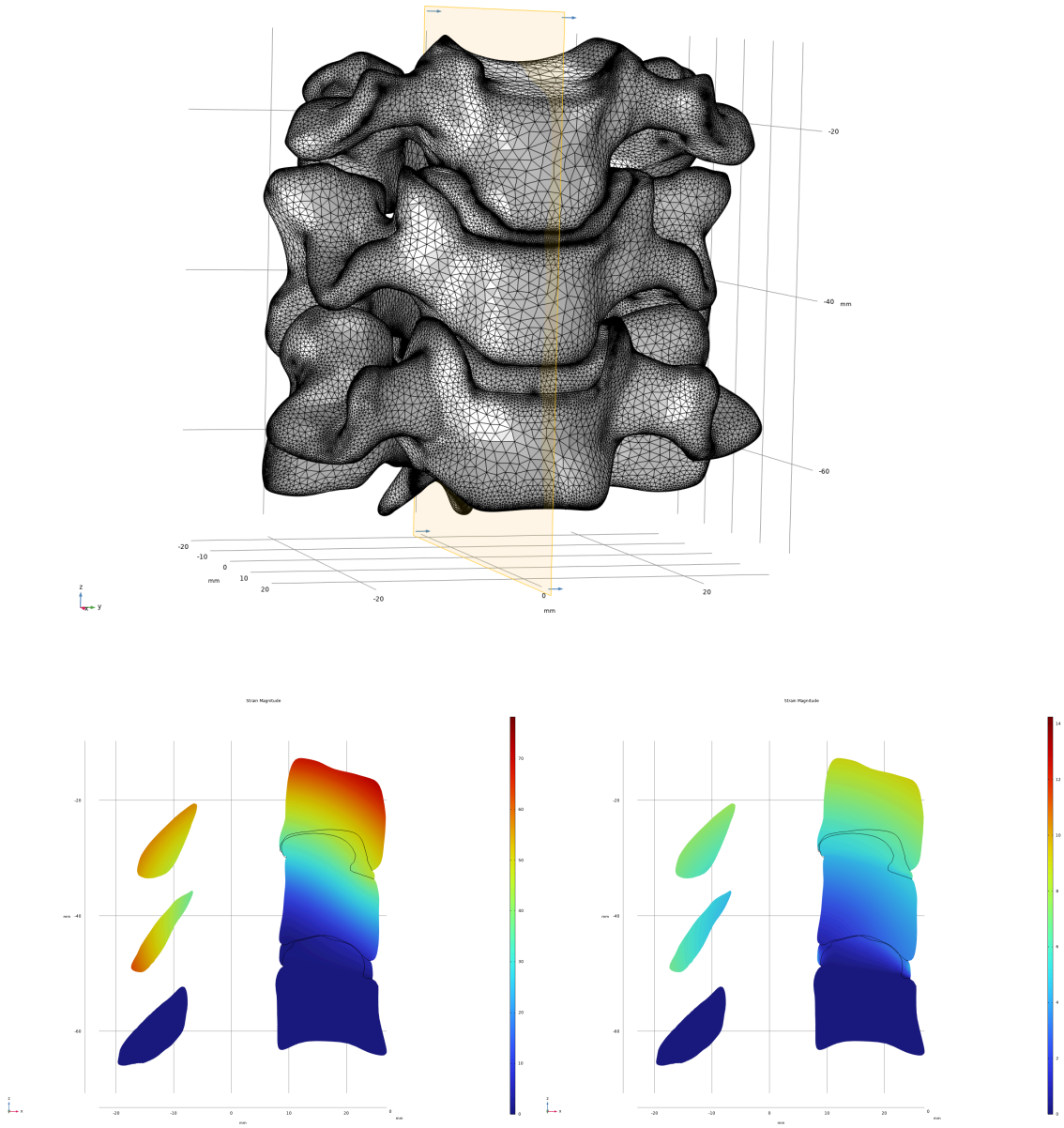

Figure 11: (Top Image) Slice of the vertebral system taken from the XZ direction to visualise strain magnitude. (Left Image) Contains no implant (Right Image) Contains the cement implant (Geometry 1).

Discussion

Cement implantation serves as an effective stress distribution tool to alleviate the stress entering an affected structurally compromised vertebrae. The added risk of this is the increased stresses experienced by surrounding vertebrae during common load scenarios. The V3 adjacent vertebra is more susceptible to

fracture in these scenarios where V1 is a fixed parameter. If V1 were not a fixed parameter or was able to carry more of the load before beginning to surmise to zero then more accurate stress loads can be calculated. Under the current model conditions V3 is most likely to generate stress concentrations not only due to its role as the boundary load condition, but also because it experiences elevated stress concentrations, particularly along the inferior endplate. Clinically, this trend is well supported, with 20%–25% of additional fractures occurring as failures of the inferior endplate of the vertebra above the treated level (23). Furthermore, the likelihood of such fractures increases with greater volumes of cement augmentation, which amplify stiffness mismatch and stress concentration at this interface (23).

Despite the progress demonstrated in this work, particularly in building more accurate simulations informed by prior models, significant challenges remain when vertebrae are extracted directly from patient DICOM data. The immediate limitation is the loss of unique skeletal features during the "reconstruction" process required to repair holes, fill voids, and correct artifactual geometries. Although the reconstructed vertebra retains patient-specific bone density through the use of CT-derived Hounsfield unit based density mapping, this advantage comes at the cost of eliminating the natural cortical trabecular dual-domain structure that has become standard in spinal modeling. This homogenization can obscure the mechanical and structural distinctions at the cortical trabecular interface, which are critical for accurately representing load transfer and failure behavior. However, this limitation may be partially correctable through the incorporation of higher sensitivity imaging modalities such as DEXA or micro-CT which offer improved density resolution (50). These approaches could enable more precise isolation and reconstruction of the cortical–trabecular boundary, thereby restoring aspects of the dual-domain architecture while preserving the benefits of patient-specific density mapping. The resulting homogenized density field leads to less accurate biomechanical simulations. This model also neglects the visceral and muscle forces keeping it inline with previous spinal studies though the inclusion of this dynamic system will be imperative in fully understanding the true distribution of stresses within the spinal system [49].

A logical next step for strengthening this model would be to establish statistical relevance by integrating the model's predicted fracture pattern with secondary fracture clinical data. This would be possible with additional EPIC data and a subsequent clinical study. By correlating simulated fracture risk with real patient outcomes, the hypothesis could gain empirical support and move toward clinical validation. This system could evolve into a pre-operative decision-support tool, enabling surgeons to identify patients at elevated risk for adjacent vertebral fractures and tailor augmentation strategies accordingly, potentially reducing complication rates and improving long term spinal stability.

Furthermore, the model highlights the importance of cement morphology and stiffness mismatch in driving these stress patterns. Increased global system stress, despite improved local stability, underscores a key tradeoff in current vertebroplasty approaches: mitigation of local failure at the expense of increased risk to surrounding structures. This reinforces the need for optimization of cement material properties and geometry to better approximate native bone behavior and reduce adverse load transfer effects.

Future work should focus on integrating higher-resolution imaging and multimodal datasets, as well as correlating model predictions with clinical outcomes. In conclusion, this work demonstrates the effectiveness of CT-driven finite element analysis as a tool for predicting stress redistribution in vertebral systems following cement augmentation. By incorporating patient-specific geometries from DICOMs rather than relying on idealized models, the simulations capture clinically relevant variations in anatomy and cement morphology, enabling a more accurate representation of biomechanical behavior under compressive loading. Ultimately, the framework developed in this study has the potential to evolve into a clinically relevant decision-support tool, enabling patient-specific risk assessment and improved treatment planning for vertebral augmentation procedures.

References:

1. Johnell O, Kanis JA. An estimate of the worldwide prevalence and disability associated with osteoporotic fractures. *Osteoporos Int.* 2006;17(12):1726–1733. doi:10.1007/s00198-006-0172-4

2. Burge R, Dawson-Hughes B, Solomon DH, Wong JB, King A, Tosteson A. Incidence and economic burden of osteoporosis-related fractures in the United States, 2005–2025. *J Bone Miner Res.* 2007;22(3):465–475. doi:10.1359/jbmr.061113

3. Galibert P, Deramond H, Rosat P, Le Gars D. Preliminary note on the treatment of vertebral angioma by percutaneous acrylic vertebroplasty. *Neurochirurgie.* 1987;33(2):166–168.

4. Heini PF. The current treatment—a survey of osteoporotic fracture treatment. *Osteoporos Int.* 2005;16(Suppl 2):S85–S92. doi:10.1007/s00198-004-1754-9

5. Kamio T, Sakai T, et al. DICOM segmentation and STL creation for 3D printing: software comparison for osseous anatomy. *3D Print Med.* 2020;6:17. doi:10.1186/s41205-020-00075-5

6. American College of Radiology (ACR). ACR Appropriateness Criteria®: Management of Vertebral Compression Fractures. Reston (VA): American College of Radiology; 2022.

7. Miao KH, Miao JH, Belani P, et al. Radiological diagnosis and advances in imaging of vertebral compression fractures. *J Imaging.* 2024;10(10):244. doi:10.3390/jimaging10100244

8. Khan MA, Jennings JW, Beaman FD, et al. ACR Appropriateness Criteria® management of vertebral compression fractures: 2022 update. *J Am Coll Radiol.* 2023;20(5 Suppl):S102–S124. doi:10.1016/j.jacr.2023.01.024

9. Fisher CG, DiPaola CP, Ryken TC, et al. A novel classification system for spinal instability in neoplastic disease. *Spine (Phila Pa 1976).* 2010;35(22):E1221–E1229. doi:10.1097/BRS.0b013e3181e16ae2

10. Kanis JA, McCloskey EV, Johansson H, et al. Interpretation and use of FRAX in clinical practice. *Osteoporos Int.* 2011;22(9):2395–2411. doi:10.1007/s00198-011-1713-z

11. Shepherd JA, Schousboe JT, Broy SB, et al. Advanced analysis techniques improve clinical utility of DXA. *J Clin Densitom.* 2017;20(3):290–303. doi:10.1016/j.jocd.2017.06.005

12. Lewiecki EM. DXA: Clinical applications and interpretation. *Curr Osteoporos Rep.* 2010;8(2):77–83. doi:10.1007/s11914-010-0014-0

13. Binkley N, Adler RA, Bilezikian JP, et al. Official positions of the ISCD on bone densitometry. *J Clin Densitom.* 2019;22(4):489–495. doi:10.1016/j.jocd.2019.07.001

14. Fourney DR, Schomer DF, Nader R, et al. Percutaneous vertebroplasty and kyphoplasty for painful vertebral fractures in cancer patients. *J Neurosurg Spine.* 2003;98(1):21–30. doi:10.3171/spi.2003.98.1.0021

15. Cotten A, Dewatre F, Cortet B, et al. Percutaneous vertebroplasty for osteolytic metastases and myeloma. *Radiology.* 1996;200(2):525–530. doi:10.1148/radiology.200.2.8685361

16. Wallace AN, Tomasian A, Vaswani D, et al. Radiation therapy or radiofrequency ablation combined with vertebral augmentation. *J Vasc Interv Radiol.* 2015;26(1):136–143.e1. doi:10.1016/j.jvir.2014.09.015

17. Patel AA, Singh K, Kurland A. The role of vertebral augmentation in metastatic spinal disease. *Curr Rev Musculoskelet Med.* 2020;13(4):490–497. doi:10.1007/s12178-020-09669-3

18. Black DM, Delmas PD, Eastell R, et al. Once-yearly zoledronic acid for osteoporosis. *N Engl J Med.* 2007;356(18):1809–1822. doi:10.1056/NEJMoa067312

19. Khosla S, Burr D, Cauley J, et al. Bisphosphonate-associated osteonecrosis of the jaw. *J Bone Miner Res.* 2007;22(10):1479–1491. doi:10.1359/jbmr.0707onj

20. Fizazi K, Lipton A, Mariette X, et al. Denosumab versus zoledronic acid in bone metastases. *J Clin Oncol.* 2011;29(9):1125–1132. doi:10.1200/JCO.2010.31.3304

21. Russell RGG. Bisphosphonates: The first 40 years. *Bone.* 2011;49(1):2–19. doi:10.1016/j.bone.2011.04.022

22. Guise TA, Mohammad KS, Clines G, et al. Mechanisms of osteolytic and osteoblastic metastases. *Clin Cancer Res.* 2006;12(20 Pt 2):6213s–6216s. doi:10.1158/1078-0432.CCR-06-1003

23. Lewis G. Injectable bone cements for vertebroplasty and kyphoplasty. *J Biomed Mater Res B Appl Biomater.* 2006;76B(2):456–468. doi:10.1002/jbm.b.30435

24. Boger A, Bohner M, Heini P, Schneider E. Injectable low modulus PMMA bone cement. *J Biomed Mater Res B Appl Biomater.* 2008;86B(2):474–482. doi:10.1002/jbm.b.31044

25. Seesala VS, Sheikh L, Basu B, Mukherjee S. PMMA bone cement review. *ACS Biomater Sci Eng.* 2024;10(10):5939–5959. doi:10.1021/acsbiomaterials.4c00779

26. Frontiers in Materials. Modified PMMA and calcium-based bone cement. *Front Mater.* 2022;9:912713. doi:10.3389/fmats.2022.912713

27. Ramanathan S, et al. Poly(methyl methacrylate) in orthopedics. *Polymers.* 2024;16.

28. Karpiński R, Szabelski J. PMMA with glassy carbon. *J Funct Biomater.* 2025;16(7):254. doi:10.3390/jfb16070254

29. Li L, Cao H, Guan J, et al. Fracture properties of PMMA. *Polymers.* 2022;14(17):3589. doi:10.3390/polym14173589

30. Lee C. Mechanical properties of bone cement. In: *Bone Cement.* Springer; 2003:37–51. doi:10.1007/3-540-28924-0_6

31. Wang Y, Huang F, Chen L, et al. Intravertebral pressure during vertebroplasty. *Pain Physician.* 2013;16(4):E411–E418

32. Lee SH, Kim YH, Kim YB, et al. Intraosseous pressure during cement injection. *Clin Orthop Surg.* 2022;14(4):505–511. doi:10.4055/cios21097

33. Deramond H, Wright NT, Belkoff SM. Temperature during vertebroplasty. *Bone.* 1999;25(2 Suppl):17S–21S. doi:10.1016/S8756-3282(99)00107-2

34. Lai PL, Chen LH, Niu CC, et al. Cement leakage and thermal injury. *BMC Musculoskelet Disord.* 2011;12:116

35. Szoradi GT, et al. Thermal necrosis from PMMA polymerization. *Appl Sci.* 2024;14

36. Dickey BT, Tyndyk MA, Doman DA, Boyd D. Stress distribution after augmentation. *J Mech Behav Biomed Mater.* 2012;5:283–290

37. Zhang Y, Li X, Wang Y, Chen X. FE evaluation of vertebral augmentation. *J Biomech.* 2024;163:112147

38. Chabarova O, Selivonec J, Menendez Hurtado A. Osteoporotic vertebra modeling. *Bioengineering.* 2024;11(5):507

39. Wiczenbach T, Pachocki L, Daszkiewicz K, et al. Lumbar spine FE model. *PeerJ.* 2023;11:e15805

40. Dreischarf M, Zander T, Shirazi‐Adl A, et al. Lumbar spine model comparison. *J Biomech.* 2014;47(8):1757–1766

41. Barekar SS, Sarawade SS, Kumar N. Mechanical properties of bone. *Multimed Tools Appl.* 2024;84:1359–1383

42. Hong J, Cha H, Park Y, et al. Properties of trabecular bone. In: *Med Biomed Eng Comput Conf.* 2007:274–277

43. Zimmermann EA, Schaible E, Gludovatz B, et al. Cortical bone behavior. *Acta Biomater.* 2011;7(4):1732–1739

44. Bittner‐Frank M, Reisinger AG, Andriotis OG, et al. Bone properties vs BMD. *Bone Rep.* 2020;12:100254

45. Jimenez‐Palomar I, Shipov A, Shahar R. Osteoporotic bone mechanics. *J Mech Behav Biomed Mater.* 2015;49:140–150

46. Yang H, Jekir MG, Davis MW, Keaveny TM. Disc modulus and vertebral stress. *J Biomech Eng.* 2016;138(2)

47. Elliott DM, Setton LA. Annulus fibrosus tensile behavior. *J Biomech Eng.* 2001;123(3):256–263

48. McMorran JG, Gregory DE. Loading rate in spine injury. *Med Eng Phys.* 2021;93:1–7

49. Tariq A. Intradiscal pressures in daily activities. 2010

50. Nieuwenhuijse MJ, Muijs SPJ, van Erkel AR, Dijkstra PDS. Vertebroplasty versus conservative therapy. *AJNR Am J Neuroradiol.* 2012;33(7):1305–1310. doi:10.3174/ajnr.A2964